Received February 2002
Revised July 2003
Accepted September 2003

Mathematical simulation of surface wave created in a mold due to submerged entry nozzle

Sukanta K. Dash and Swasti Sunder Mondal
Department of Mechanical Engineering, Indian Institute of Technology, Kharagpur, India
Satish K. Ajmani
Research and Development Division, Tata Steel, Jamshedpur, India

Keywords *Numerical analysis, Wave properties*

Abstract *Two-dimensional numerical simulations have been performed using a finite volume method that employs unstructured grids with cell-wise local refinement and an interface-capturing scheme to predict the shape of the free surface, thus simulating the surface wave that is created in a mold due to the flow from the submerged entry nozzle (SEN). Simulation has been done for 1:6.25 aspect ratio of the mold having a height of 2 m with parallel rectangular ports as well as 15° upward and downward ports. It has been found that for low inlet velocity of the SEN (< 1 m/s) the maximum wave amplitude of the surface remains below 12 mm and no outside air is entrapped by the wave to form a bubble. However, for high inlet velocity (2 m/s or more) there is considerable fluctuations on the free surface and the maximum wave amplitude shoot up beyond 70 mm at the start up and slowly falls to about 30 mm entrapping air bubbles from the surroundings. The movement of the air bubble within the mold and its rise to the free surface where it subsequently collapses has been captured well in the numerical simulation. The overall shape of the free surface matches well, excepting the initial transience, with that of the experimentally observed free surface, although the free surface never attains a perfect steady shape neither in the experiment nor in the numerical simulation due to its continuous oscillation and breaking.*

Nomenclature

c = volume fraction of the fluid
k = turbulent kinetic energy
p = pressure
t = time
U = mean velocity
x = coordinate for measure of distance
ρ = density of the fluid
μ = coefficient of viscosity
ν = kinematic viscosity
$\overline{u_i u_j}$ = average turbulent stress
ε = rate of dissipation of turbulent kinetic energy
σ = surface tension coefficient
ϕ = either k or ε

Subscripts

i, j, k = three Cartesian coordinate directions x, y and z
1 = Fluid 1 (liquid)
2 = Fluid 2 (gas)

The author (Sukanta K. Dash) is grateful to Tata Steel for supporting this research work. The author also expresses his sincere gratitude to the Alexander von Humboldt Foundation who financially supported him in obtaining the CFD software "COMET" and the highend PC using which the present computations were carried out.

International Journal of Numerical Methods for Heat & Fluid Flow
Vol. 14 No. 5, 2004
pp. 606-632

0961-5539
DOI 10.1108/09615530410539946

Introduction

In recent times, steel makers are aiming for high quality steel with improved productivity. As a result the casting speed of the liquid steel has to be high which brings several other problems in the mold leading to loss of quality. This conflicting requirement has brought in the need to study surface wave or computation of free surface in the mold. In a continuous slab caster, a higher casting speed leads to lot of fluctuations in the free surface of the liquid level in the mold. This fluctuation in the free surface with the association of frequent vortex entraps the slag and the surrounding air, which can spoil the quality of the steel. Therefore in recent times, lot of attention and effort has been directed towards the study of the free surface in a mold and its measurement. Effort has been made to minimize the maximum amplitude of the surface wave by putting electromagnetic field around the free surface of the mold, which is shown to be an expensive arrangement. Lot of experimental and theoretical works has been reported by Andrzejewski *et al.* (1992), Ferritti and Podrini (1985), Gupta and Lahiri (1992, 1993), Gupta *et al.* (1991), Matsuhita *et al.* (1988), Nakato *et al.* (1984), Qinglin (1993), Robertson *et al.* (1986), Szekely and Yadoya (1972) and Thomas *et al.* (1990) to assess the flow pattern in the mold but no effort has been made to arrive at a numerical prediction of surface wave fluctuation due to the presence of the flow field in the mold, in the light of present numerical computation. In the past, researchers have put attention to compute the flow field in the mold without trying to compute the shape of the free surface, simply because such computational techniques were not available. Most of the work with free surface was experimental where actual measurement of the surface wave can be found in the work of Andrzejewski *et al.* (1992), Gupta and Lahiri (1993) and Matsuhita *et al.* (1988). It should be noted that accurate measurement of the surface wave needs high speed camera and image analyzer and an elaborate experimental setup which can be very expensive. But with the present numerical technique prediction of surface wave can be accurate and this can be simulated for any complex geometrical shape due to the use of unstructured grid.

Panaras *et al.* (1998) have used a volume of fluid (VOF) technique to predict the surface wave in a mold due to submitted entry nozzle (SEN) and they have suggested a criterion to adopt maximum velocity so that instability can be avoided on the free surface. Anagnostopoulos and Bergeles (1999) and Theodorrakakos and Bergeles (1998) in their work have computed the free surface of two fluids (water and oil) in a mold by the VOF method but they have not shown the entrapment of air bubble or the entrapment of the lighter fluid in the heavier one, simply because the treatment of VOF method in their study is not capable of handling overturning shapes of the free surface. Moreover, they have not solved the species continuity equation (to represent the volume fraction of a desired fluid) and have not incorporated the forces due to surface

tension, which can cause the free surface to change a lot, in their modeling. Such effects are taken into account in the present numerical investigation.

Literature survey shows that – to our knowledge – there are no published results on numerical simulations of surface wave in a mold created due to the flow from the SEN having a direct comparison with experimental findings. The reason is that methods, which allow simulations of two-fluid flow with complicated free-surface pattern have only recently emerged (Lafaurie *et al.*, 1994; Muzaferija and Peric, 1999; Ubbink, 1997. One such method developed by Muzaferija and Peric (1999) has been successfully used in this study to predict the surface wave, the entrapment of bubbles through the free surface and their subsequent movement in the mold following further collapse and coalescence of the bubbles.

Problem description

The experimental setup is shown schematically in Figure 1 and symmetry has been exploited to show half of the setup. The SEN as well as the mold are made from Perspex glass. The diameter of the SEN is 25 mm and the wall thickness is 10 mm. The port opening is 33 mm and the submergence depth is kept at 125 mm from the free surface, which can be visualized from Figure 1. The width of the mold is 500 mm and thickness 80 mm, which keeps the aspect ratio of the mold at 1:6.25. The height of the mold is 2 m. Initially water is filled in the mold up to a level so that the submergence depth of the SEN is 125 mm. Then water is allowed to flow into the SEN from a reservoir (called tundish) through a stopper rod arrangement and the reservoir is fed in by water through a pump.

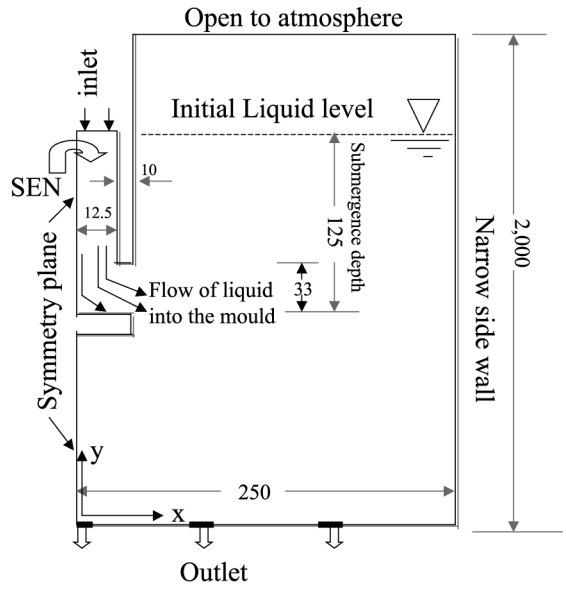

Figure 1.
Schematic view of the SEN in the mold, all shaded lines represent walls, all dimensions in millimeter

The level in the reservoir is kept constant by adjusting the flow rate into it. Slowly the flow rate of water into the SEN and flow rate out of the mold through the outlets at the bottom of the mold settles to a steady value. There are five openings at the bottom of the mold, which are connected through outlet pipes of 10 mm diameter to a large buffer. In the simulation we use two full outlets and one half outlet in order to force symmetry. The half outlet is 5 mm in width and is created near the symmetry plane. All other portion at the bottom of the mold is a solid wall. In Figure 1, the arrows represent the outlets and the rest of the portions are wall.

The objective is to compute the free surface for a particular submergence depth, with a specified inlet velocity to the SEN for which case an exact snapshot from the experiment can be taken and a possible comparison with the numerical simulation can be made. There can be variations in the port angle of the SEN. In the present study, we have taken a parallel port (0°), SEN as well as 15° up and 15° downward port SEN but results for only parallel port SEN will be discussed because the inclined port results are not much different from the parallel port result. To start with, the level in the mold is such that the submergence depth is 125 mm. But when the pump starts the level changes too fast and adjustments in the flow rate are required to keep the submergence depth at a specified value. This operation takes time and this is the reason why the initial transience could not be matched with the experimental findings. In a mathematical simulation the initial level of liquid can be specified at any value and the inlet and outlet flows can be specified to a desired value; so a smooth transient can be simulated but unfortunately this could not be controlled in the actual experiment for which the initial transience could not be matched with that of the experiment. However, the surface wave is repetitive in nature and barring the initial transience a wave pattern can be found out with time, which can be favorably compared with the numerical simulation.

From experimental evidence it has been found that there is no significant change in the wave amplitude in the direction of the narrow sidewall. So in order to keep the computational time low, a two-dimensional simulation has been undertaken to simulate the free surface in the mold. Normally a simulation of free surface will require very fine grid near the free surface and a three-dimensional computation could have taken a huge amount of control volumes (CVs) (and hence time) as compared to the same resolution that is used in a two-dimensional simulation (Figure 2).

Governing equations

The finite volume method for incompressible viscous flows with free surface is described briefly in detail by Muzaferija and Peric (1999). The starting point are the conservation equations for mass, momentum and scalar quantities (e.g. energy or chemical species) in their differential form.

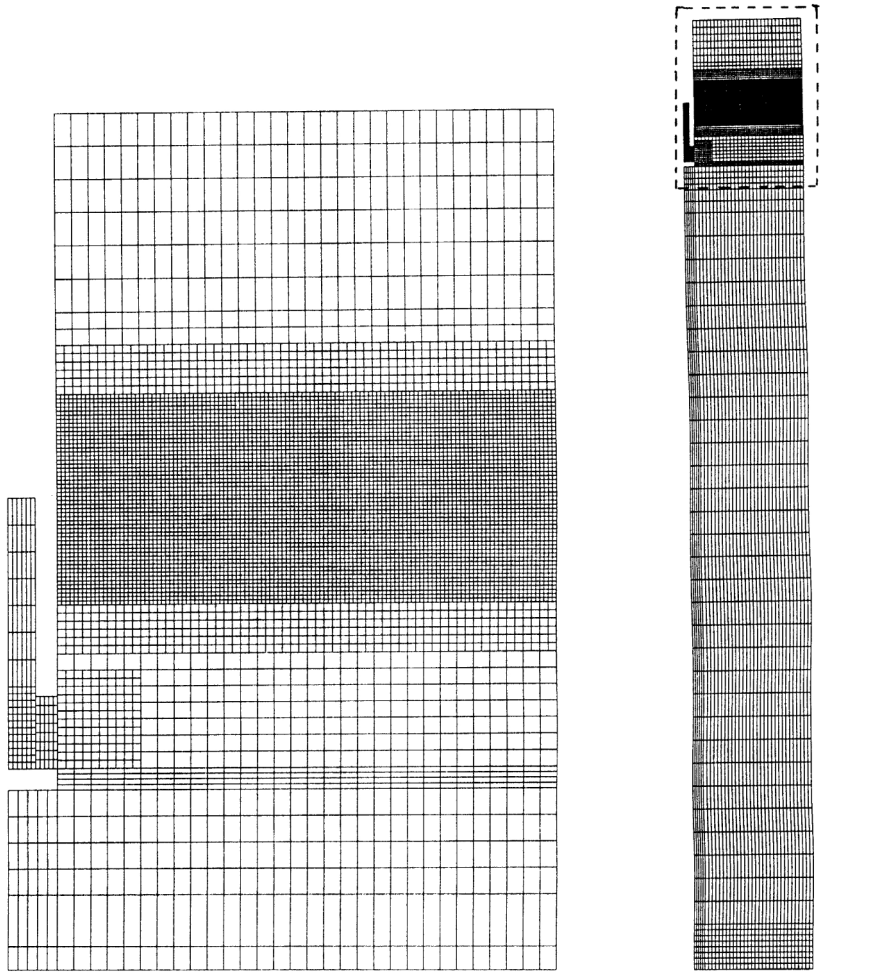

(b) Expanded view of the dashed line portion containing the SEN and initial liquid level

(a) Full scale numerical set up

Figure 2.
Arrangement of control volumes in the SEN and mold

Continuity

$$\frac{\partial \rho}{\partial t} + \frac{\partial}{\partial x_i}(\rho U_i) = 0 \tag{1}$$

Momentum

$$\frac{\mathrm{D}(\rho U_i)}{\mathrm{D}t} = -\frac{\partial p}{\partial x_i} + \frac{\partial}{\partial x_j}\left[\mu\left\{\frac{\partial U_i}{\partial x_j} + \frac{\partial U_j}{\partial x_i}\right\} - \overline{\rho u_i u_j}\right] + \rho g + F_\sigma \tag{2}$$

Turbulent kinetic energy

$$\frac{\mathrm{D}(\rho k)}{\mathrm{D}t} = \mathrm{D}_k + \rho P - \rho\varepsilon \tag{3}$$

Rate of dissipation of k

$$\frac{\mathrm{D}(\rho\varepsilon)}{\mathrm{D}t} = \mathrm{D}_\varepsilon + C_1\rho P\frac{\varepsilon}{k} - C_2\frac{\rho\varepsilon^2}{k} \tag{4}$$

where

$$\overline{u_i u_j} = \frac{2}{3}k\delta_{ij} - \nu_t\left(\frac{\partial U_i}{\partial x_j} + \frac{\partial U_j}{\partial x_i}\right), \quad \nu_t = \frac{C_\mu k^2}{\varepsilon}$$

$$D_\phi = \frac{\partial}{\partial x_j}\left[\left(\mu + \frac{\mu_t}{\sigma_\phi}\right)\frac{\partial\phi}{\partial x_j}\right], \quad P = -\overline{u_i u_j}\frac{\partial U_i}{\partial x_j}$$

Constants used in the k-ε model are:

$$C_1 = 1.44, \quad C_2 = 1.92, \quad \sigma_\mathrm{c} = 1.0$$

$$\sigma_k = 1.0, \quad \sigma_\varepsilon = 1.3, \quad C_\mu = 0.09$$

A single momentum equation (equation (2)) is solved throughout the domain, and the resulting velocity field is shared among the phases. The momentum equation, shown in equation (2), is dependent on the volume fractions of all phases through the properties ρ and μ.

Surface tension and interface capturing

Interface-capturing method and high-resolution interface capturing (HRIC) scheme (Muzaferija and Peric, 1999) have been used to simulate the free-surface effects. In addition to the conservation equations for mass and momentum, a transport equation for void fraction of the liquid phase c has been introduced:

$$\frac{\partial c}{\partial t} + U\cdot\nabla c = 0 \tag{5}$$

The grid extends to both liquid and gas phases; the void fraction c is set equal to 1 for CVs filled by liquid and 0 for CVs filled by gas. Both fluids are treated as a single effective fluid whose properties vary in space according to the volume fraction of each phase, i.e.:

$$\rho = \rho_1 c + \rho_2(1-c), \quad \mu = \mu_1 c + \mu_2(1-c) \tag{6}$$

where subscripts 1 and 2 denote the two fluids (e.g. liquid and gas).

The effects of surface tension at the interface between two fluids are taken into account through a body force as a function of the volume fraction c, which is achieved by introducing the continuum surface force (CSF) model (Brackbill *et al.*, 1992). The CSF model uses the smoothed field of c to define a unit vector normal to the interface with the help of the gradient vector of c; the divergence of this unit vector defines the curvature of the interface, κ. The surface tension force per unit volume (F in equation (2)) and the curvature can thus be expressed as:

$$F_\sigma = \sigma \frac{\rho \kappa \nabla c}{\frac{1}{2}(\rho_1 + \rho_2)} \quad \kappa = -\nabla \cdot \left(\frac{\nabla c}{|\nabla c|} \right) \tag{7}$$

where σ is the surface tension coefficient and ρ is the volume averaged density computed from equation (6). Equation (7) shows that the surface tension source term for a cell is proportional to the average density in the cell.

Air bubble model

When a bubble is entrapped in the liquid it experiences three kinds of forces on it apart from its own weight. One is the surface tension force at the interface, the second one is the viscous force on the surface as well as everywhere inside the bubble and the third is the surrounding pressure force on it. Owing to incorporation of a continuum surface force model as per equation (2) we take care of the viscous force and the surface tension force acting on any cell at any moment. The pressure gradient force is always present as it is imbedded in the momentum equation (2). So inherently the momentum equation has all the required components in it to describe the bubble dynamics when we incorporate a continuum surface force model. So separate equations describing bubble physics and its movement are not required as it is already imbedded in equation (2). The entrapment of a bubble is activated when the surface overturns and intersects itself entrapping the surrounding air into the liquid. No separate activation mechanism is required in the numerical model as the velocity field is computed for a single fluid with varying local properties. If a bubble is present then the cells will have a value of $c = 0$ and the boundary of the bubble will have a value of c lying between 0 and 1 and the physical properties of the local fluid will be computed according to equation (6) for all those cells having a value of c between 0 and 1. Velocity is computed everywhere and the velocity of the interface is also computed time to time. So the movement of the interface or the bubble can be tracked with time. The present model can therefore describe the entrapment of air bubble in the liquid and its movement in the liquid as well as its coalescence or fragmentation.

Boundary conditions

The set of differential equations (1)-(5) have been solved with a set of realistic boundary conditions. The inlet is prescribed as a known boundary condition

where the velocity normal to the boundary has been prescribed to a pre-defined value of 3.0 m/s for the experiment of Gupta and Lahiri so that the average port exit velocity is of the order of 1.94 m/s for which the experiment was conducted. In our present experiment, the inlet velocity is set to 2 m/s (or 0.84 m/s for low velocity case) where we have done the study on bubble entrapment and its movement. The turbulence intensity is set to 2 per cent at the inlet from which the inlet values of k and ε could be specified (for a detail specification of this, see Jha and Dash (2002)). The outlet is given a zero gradient condition for all the variables. The wall is specified with a equilibrium log law wall function for the turbulent quantities from where k and ε are computed from the wall functions (Jha Pradeep and Dash Sukanta, 2002). The surface open to atmosphere at the top of the domain is given a pressure boundary condition where the pressure is set to be atmospheric. At the symmetry plane, zero gradient conditions in a direction normal to the symmetry plane for all the variables are used. At the wall zero gradient condition for the volume fraction, c has been used because the quantity c, cannot diffuse into the wall. With all these set of boundary conditions one initial condition for all the variables is needed to start the solution.

Initial condition

At time $t = 0$ all velocity components are set to 0, except the value at the inlet where the normal velocity into the domain is set to a prescribed value. All the turbulent quantities are initialized to zero everywhere in the domain except at the inlet where they are given a pre-defined value of 2 per cent intensity. At the inlet c is set to zero (for air) as we are solving for water as the primary phase and air as the secondary phase. Up to the initial water level in the solution domain, the value of c is set to be 1 and else where the value of c is kept at 0 signifying that the rest of the domain is filled with air to start with.

Properties of the fluids used in the simulation

In the numerical simulation only two fluids, water and air, are used. The properties of the two fluids taken for the simulation are as shown in Table I.

Numerical solution methodology

The solution domain is subdivided into a finite number of non-overlapping CVs: in the center of each CV lies the computational point at which the known

Property	Water	Air
ρ	988.3 kg/m^3	1.225 kg/m^3
σ	0.073 N/m	–
μ	0.001013 Pa s	1.8×10^{-5} Pa s

Table I.

quantities are specified and the unknown variables are to be computed. Local refinement was used to achieve finer resolution in regions of rapid change of the variables, as shown in Figure 2. The CVs are treated as polyhedra and can have an arbitrary number of neighbors (unstructured grids).

Equations (1)-(5) are applied to each CV and then discretized, leading to one algebraic equation per CV in which variables from immediate neighbors also feature. All integrals are approximated using midpoint rule, i.e. the function to be integrated is evaluated at the center of the integration domain and multiplied by the area, volume or time interval over which the integration takes place. In order to evaluate the function at the center of the integration domain, one needs to introduce further approximations: interpolation and differentiation. In space, linear interpolation is used, while in time either linear or quadratic shape functions are used. The diffusive fluxes require that the derivatives in the direction normal to CV faces be computed at each cell-face center; these are obtained from linear shape functions with the help of least-squares method or Gauss-theorem. The integration in time is fully implicit (first-order Euler implicit method). The spatial integration is also of either first or second order, depending on the approximation of convected variable in convective fluxes (upwind or central differencing, or a blend of the two). In the present computation first-order up winding scheme was adopted for the convective fluxes with a blending factor of 0.5. In order to keep the computational molecule limited to cell center node and centers of nearest neighbor cells, the deferred-correction approach is used: low-order approximations which use only nearest neighbors are used to construct the coefficient matrix, and the difference between the desired approximation and the low-order one is computed explicitly from the values obtained in the previous iteration and added to the source term on the right-hand side of the equation. More details on individual steps in the discretization procedure can be found in Muzaferija and Peric (1999).

In order to calculate the pressure field and to couple it properly to the velocity field, a pressure-correction method of SIMPLE-type (Patankar and Spalding, 1972) is used. Velocities computed from momentum equations using pressure from previous iteration step are corrected to enforce mass conservation, and the correction to cell-face velocity is proportional to the gradient of pressure correction, leading to a Poisson-type pressure-correction equation. Turbulence is taken into account by solving two additional transport equations for turbulent kinetic energy k and its dissipation rate ε and adding an eddy viscosity (computed with help of these two quantities) to the molecular viscosity. When solving equation (5), a special interpolation method is used to compute the cell-face value of the volume fraction c (HRIC-scheme, Muzaferija and Peric, 1999), which is designed to keep the interface sharp (i.e. avoid spreading due to numerical diffusion) and to maintain c bounded (i.e. c is not allowed to become less than zero or greater than unity). This is achieved by

blending the upwind and downwind approximations, with blending factor being a function of the local profile of c, the orientation of interface relative to cell-face, and the local Courant number. The following equations show how the cell-face value of volume fraction c is computed at the cell-face j according to the HRIC scheme.

$c_j = c_j^{**}(c_D - c_U) + c_U$ where $c_j^{**} = c_j^{*}\sqrt{\cos(\theta)} + c_C\left(1 - \sqrt{\cos(\theta)}\right)$ and θ represents the angle between the normal to the interface (found out by the gradient vector of c) and the normal to cell-face (Figure 3).

$$c_j^{*} = \begin{cases} \overline{c_j} & \text{if } \mathrm{Co} < 0 \\ c_C + (\overline{c_j} - c_C)\frac{0.7-\mathrm{Co}}{0.7-0.3} & \text{if } 0.3 \le \mathrm{Co} < 0.7 \\ c_C & \text{if } 0.7 \le \mathrm{Co} \end{cases}$$

where the local Courant number is $\mathrm{Co} = v \cdot nS_j \delta t / \delta V_c$ (S_j is the surface area at j and δV_C is the volume of the cell C.

$$\overline{c_j} = \begin{cases} c_C & \text{if } c_C < 0 \\ 2c_C & \text{if } 0 \le c_C \le 0.5 \\ 1 & \text{if } 0.5 \le c_C \le 0.5 \\ c_C & \text{if } 1 \le c_C \end{cases}$$

More details on the method are available in Muzaferija and Peric (1999). It is implemented in the commercial code (Comet User Manual, n.d.), which has been used in this study.

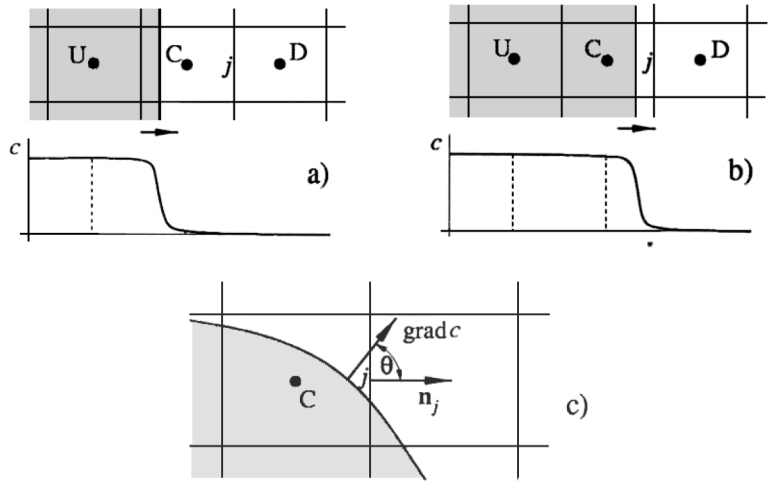

Note: Shaded portion represents presence of c, U = up stream, C = center node where c is being computed, D = down stream node

Figure 3.
On the computation of cell-face volume fraction at face j

Time step used for the integration of the equation was 0.00005 s at the start of the solution and later on it was slowly increased to 0.0001 s and then decreased to 0.00002 s when the wave was about to break and bubbles started to be entrapped in the liquid. About 2-3 iterations per time step was required for a converged solution to be achieved at each time step. The cells at the interface had a maximum size of 1.85×1.85 mm, which could capture the interface very sharp. A grid independency test on this will be discussed later in the text. Cell sizes near the port exit are kept smaller because in this region there will be considerable change in the velocity as the flow would swell into the caster. Once the flow comes into the mold there will be a recirculation zone on the south side of the port and another on the north of the port. Cell size down the port will not affect the free surface because that will be always covered with water. Whereas the cells located on the north side of the port may experience the presence of a bubble so the cells on the north of the port are to be made very fine to capture the free surface. The initial level of water is kept at the level of the inlet port and around that zone in the mold the cells are made very fine (which can be seen to very small in Figure 2(a) and (b). Again away from the interface there will be only air and the velocity change will not be very high so the cells can be made again coarser there which can be seen in Figure 2(a) and (b).

Results and discussions

The CVs employed in the simulation of free surface are shown in Figure 2. In Figure 2(a) (right side figure), the actual size of the SEN and the mold is shown. The blown up view of the upper dotted portion is shown in Figure 2(b) (left hand side picture). In the upper portion of the mold the grid has to be very fine and locally refined so that the free surface can be captured well. The initial location of the free surface is known *a priori* and hence local refinement in cells is done around this location (50 mm up and down around the initial level is refined). The minimum cell size is about 1.85 mm in that location for all the computations with an inlet velocity of 2.0 m/s. The upper part of the mold is filled with air and the local velocity is not expected to change there by a great amount, hence the grid size is kept large in this zone. A minimum cell size of 1.85×1.85 mm was found to produce grid independent solution for the free surface and bubble entrapment. Grid refinements were done near the free surface because it is expected that the value of volume fraction, c, can change significantly here; so a finer grid can capture the free surface very sharp. Grids were also refined near the outlet to capture the exit velocity properly. Table II shows the effect of grid refinement on the appearance of the first wave break up.

Initially a higher time step could be used but when the wave breaks there is a need for small time step so that the free surface can be properly captured along with the entrapment of the air bubbles.

Low inlet velocity

A simulation with an inlet velocity of 0.84 m/s was performed for both parallel port and 15° downward port SEN. The resulting surface waves (free surface) for a parallel port SEN is shown in Figure 4(a). Figure 4(b) shows the experimental snapshot for the exact case. The surface waves created in a 15° downward port are not much different from the waves created due to a parallel port. So we intend not to discuss the case of 15° downward port here. In Figure 4(a), the free surface is plotted starting from $t = 1$ to 6 s. It can be read from the figure (from the vertical millimeter scale attached to the figure) that the maximum amplitude (vertical distance between the crest and trough of the wave) $A_{\max,}$ of the wave is limited to about 9-10 mm.The scale put at the top of the figure helps to read the location of the wave in the mold. The left hand side of the nozzle wall is located at 22.5 mm from $x = 0$ line while the narrow side wall is located at 250 mm from $x = 0$. After 1 s the free surface almost attains a quasi steady state without much variation in the maximum amplitude. The shape of the free surface has been photographed from the experiment and the snapshot is shown in Figure 4(b) starting from t=1 to 6 s. It can be observed that the free surface computed from the present method matches well with that of the experiment, at least qualitatively.

It can be clearly visualized from Figure 4(a) and (b) that there is no over turning in the surface or breaking of the free surface and no entrapment of air bubble takes place for an inlet velocity of 0.84 m/s. This phenomenon is also observed in the experiment. A comparison of free surface with that of the experimental snapshot reveals that the free surface matches well with that of the experiment in later time, barring the initial transience. The initial transience of the free surface, taking place in the experiment, could not be simulated through the present computation due to initial mismatch in the inlet and outlet flow rate in the experiment, which is not known in advance. Had this been known then simulation could have been done. However, the shape of the free surface in later time qualitatively matches with that of the experimental observation very well.

Table III shows a comparison of the average maximum amplitude of the free surface with that of the experiment for an inlet velocity of 0.84 m/s.

High inlet velocity

The free surface simulations for an average inlet velocity of 2.0 m/s were made for three port angles; namely parallel port, 15° down and 15° upward port. Figure 5 shows a sequential development of the free surface with time for a

First appearance of wave break from $t = 0$ s					
No. of CV	0° port	No. of CV	15° down port	No. of CV	15° up port
5,890	0.92 s	6,270	0.96 s	6,580	1.08 s
9,870	0.95 s	9,986	0.98 s	11,240	1.10 s

Table II.

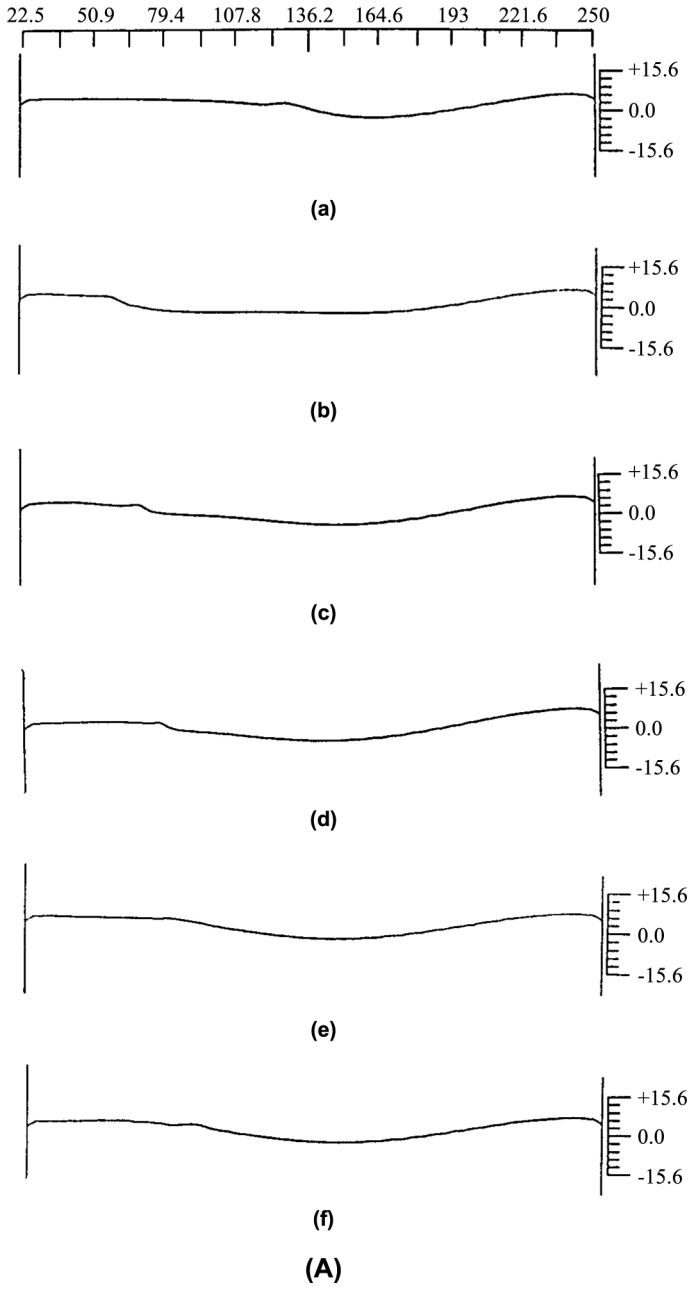

Figure 4.
(A) Development of free surface with time for a parallel port SEN with an inlet velocity of 0.84 m/s; (a) = 1 s, (f) = 6 s, with an interval of 1 s
(B) Experimental snapshot of the free surface developed with a parallel port SEN having a port exit velocity of 0.84 m/s (a) = 1 s, (f) = 6 s, with an interval of 1 s

(Continued)

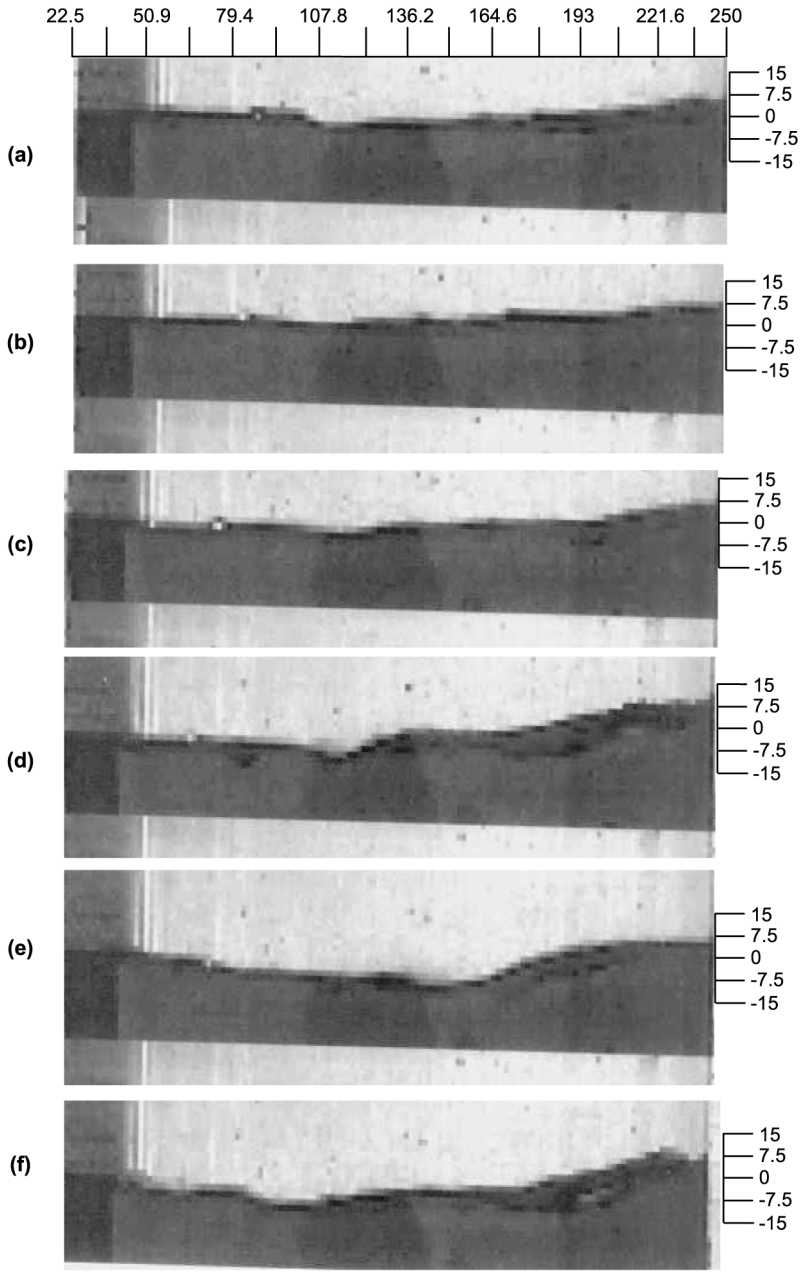

(B)

Figure 4.

parallel port SEN. It can be observed from Figure 6 that the free surface is overturning in nature and it entraps air bubble at the trough of the wave. Figure 6(a) shows the shape of the free surface at $t = 0.6$ s. The right hand side of the figure is the narrow side wall located at $x = 250$ mm and the wave amplitude can be read from the millimeter scale attached to this wall. The location and the amplitude of the free surface can also be found out from the horizontal scale attached at the top of the figure. The nozzle is located on the left hand side of the figure. The fluid comes out of the nozzle from the left side and proceeds as a jet to the right where it hits the narrow sidewall. There the fluid branches into two streams. One stream goes up and the other goes down creating two recirculation zones in the mold (Figure 10). The rising fluid carries enough kinetic energy as a result it rises up near the wall and comes to a halt because of the opposing gravity force acting on it in the downward direction. The fluid elements away from the wall have low velocity and as a result they move up to a lower height in the mold. This is the reason the free surface is always higher near the wall and it falls in height as it moves inward. The fluid elements on the free surface are always balanced by the viscous, surface tension and the gravity forces. As the free surface becomes flatter near the trough area the surface tension forces decrease (due to high radius of curvature) so the surface tries to overturn and tries to come to a new equilibrium position by turning more and enhancing the surface tension force again. But the gravity force pulls the liquid element down and as a result the free surface undergoes breaking and the breaking of the free surface entraps air bubble near the trough.

This phenomenon can be observed very well in Figure 5(b) where the free surface has broken and has entrapped an air bubble. The air bubble moves downward because the surrounding fluid pushes it down (the fluid there have downward velocity and also velocity directed towards the left wall or nozzle side wall). As the bubble moves down the local pressure on it increases and as a result it becomes smaller in size and due to the flow field it slowly moves towards the left wall (Figure 5(b)-(g)). Then the air bubble sticks to the left wall where it slowly moves up and collapses on the free surface. The bubble while collapsing moves up and comes to the free surface where it finally escapes to the ambient (Figure 5(h) and (i). In Figure 5(d), it can be seen that another wave has broken and an air bubble is entrapped in the liquid. There are many such breakings taking place in the free surface and each breaking entraps air bubble.

Table III.
A comparison of maximum wave amplitude

	Parallel port (A_{max} in mm)	15° down port (A_{max} in mm)
Experiment	8	9
Computation	9	8

Note: Experiment for parallel and 15° downward port SEN with the present computation

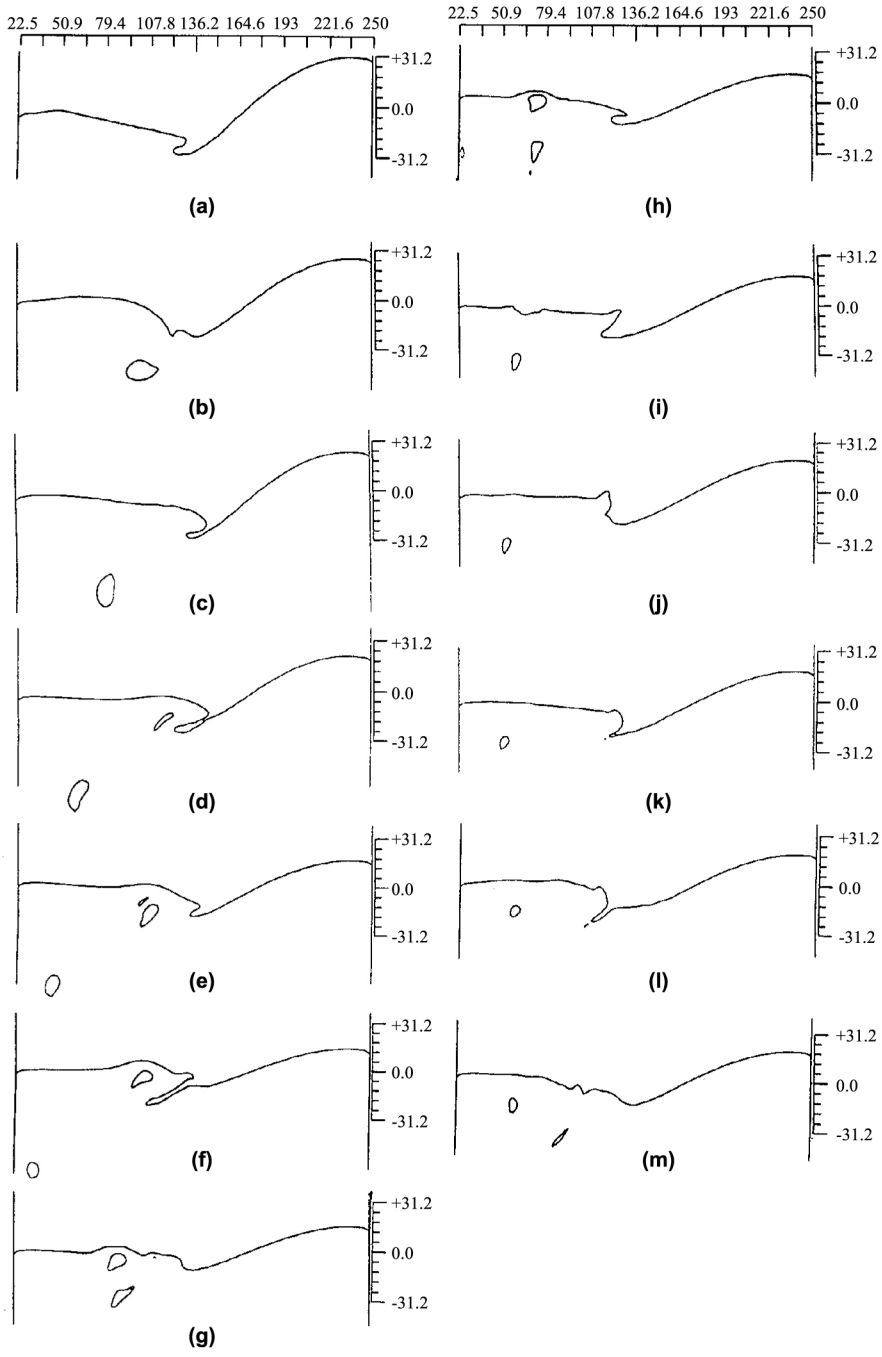

Note: (a-m) (a) = 0.6 sec, (m) = 3 sec

(*continued*)

Figure 5.
Development of free surface with time for a parallel port SEN with an inlet velocity of 2.0 m/s

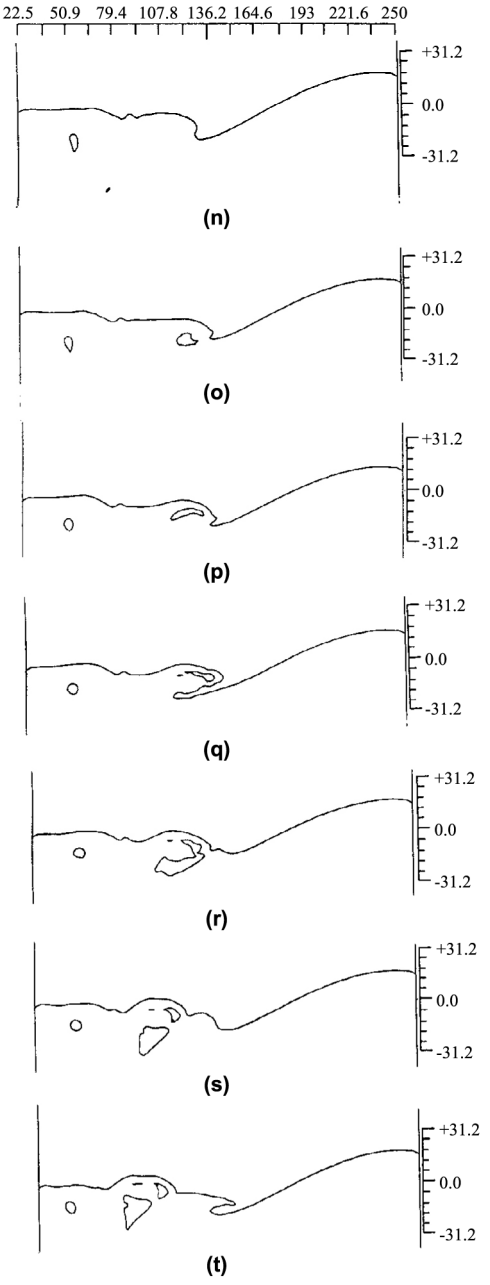

Figure 5.

Note: (n) 3.2 sec, (t) = 4.4 sec, with an interval of 0.2 sec

After the free surface has broken the maximum wave amplitude decreases suddenly and slowly again the wave amplitude increases and again the free surface breaks causing the maximum wave amplitude to decrease again. This can be seen from Figure 6 where the maximum wave amplitude is plotted with time for the parallel port SEN with an inlet velocity of 2.0 m/s.

From Figure 6 it can be observed that the wave amplitude increases from zero at $t = 0$ to a high value of 72 mm at $t = 0.95$ s where it breaks causing the amplitude to fall suddenly. In Figure 6, any sudden fall in amplitude of the wave signifies a breaking of the free surface and has been marked by an arrow. From Figure 6 it seems that the wave breaks randomly in time. But after a time of 3 s the average maximum wave amplitude remains within a certain band. It is visualized from Figures 5(a)-(m) and 6 that the free surface is continuously changing because the distance between the crest and the trough is changing with time. But the overall shape of the free surface (crest near the wall and a trough around 136 mm) looks alike although it is continuously changing with time within this band. It should be noted that the location of the crest and trough of the free surface changes with time. The location of the trough varies between $x = 110$ and 136 mm and the crest between 12 and 16 mm from the narrow sidewall. The height of the crest from the undisturbed liquid level does not vary much with time (after the initial transience) but the level of the trough varies with time. This can be read from Figure 5(a)-(m) with the help of the millimeter scale attached to the narrow sidewall.

The time when the free surface breaks can be read from Figure 6 and that can be seen from Figure 5 also in terms of the entrapment of air bubble through the free surface. In Figure 5(f), a bubble can be seen near the free surface and that has come extremely close to the free surface (Figure 5(h)) and also closer to the left wall and finally collapsed on the free surface (Figure 5(i)) leaving a dent on the free surface. Figure 5(q) shows the shape of the free surface on the verge of breaking and that has broken in the next instant (Figure 5(r)) entrapping a

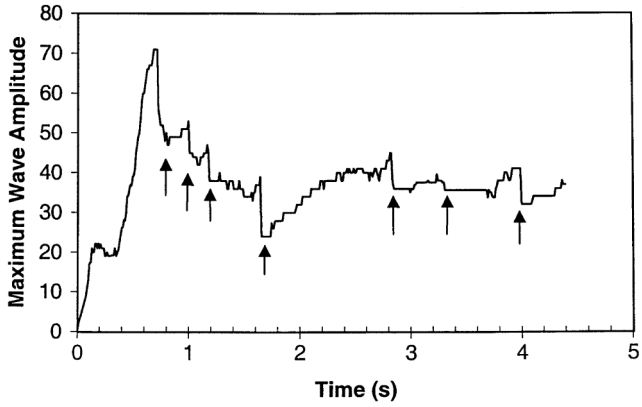

Figure 6.
Variation of maximum wave amplitude with time for a parallel port SEN (125 mm depth), arrow positions show the breaking of a wave and entrapment of air bubble

big bubble. The former bubble and the newly formed bubble have coalesced to form a bigger bubble which is unstable for which the bubble again broke into two parts in the next instant (Figure 5(s)). Again in Figure 5(t), it can be observed that the free surface is about to break. It can be expected that the bubbles, which are already entrapped by the liquid (Figure 5(q)-(s)), will escape through the free surface again by collapsing on it. Thus, Figure 5(a)-(t) shows the development of free surface with time and the breaking of the free surface with the entrapment of air bubble and movement of bubbles within the bulk of the liquid either with fragmentation or coalescence.

Similarity with experiment

The phenomenon of wave breaking for a parallel port nozzle has been explained above and it has been experimentally visualized by Gupta and Lahiri (1993). In the present experimental set-up it was difficult to arrive at an inlet velocity of more than 1.4 m/s. So the present experimental set up could not be used to study the bubble entrapment, which normally occurs at an inlet velocity of 2 m/s or more. For this reason we took the experiments of Gupta and Lahiri for a qualitative comparison with bubble entrapment. Their experimental investigation of the free surface has been numerically modeled in the present work and the grids are shown in Figure 7. Their system did not have symmetry (due to the placement of the outlet on one side of the wall) so we used a full scale model to simulate the experiment. Figure 7 also shows the boundary conditions used for the simulation and the geometrical details of their experimental setup. They used a parallel port nozzle having a circular opening with an average port exit velocity of 1.94 m/s. In order to match the average port exit velocity we put an inlet velocity of 3.0 m/s at the inlet (in the numerical computation) which gives an average port exit velocity of 1.94 m/s. Equality of mass flow rate cannot be taken into account in this simulation due to the adoption of a two-dimensional computation. The location of the free surface is at 1,072 mm from the bottom of the mold, which gives 150 mm submergence depth. The cells around this zone are refined to a size of 2.5×2.5 mm in both x and y directions.

Figure 8 shows the computed shape of the free surface at an interval of 0.04 s starting from a time of $t = 1.2$ s. It can be seen from the figure that the wave is about to break at $t = 1.32$ s (Figure 8(d)) and at $t = 1.36$ s it has broken and has entrapped an air bubble. The location of the wave break can be read from the horizontal scale while the amplitude can be read from the left hand side millimeter scale. The width of the mold in the experiment of Gupta and Lahiri is 300 mm and this can be read from the horizontal scale placed at the top of Figure 8. From Figure 9 the horizontal scale can be read from the snapshot where each division represents 10 mm (5 represents 50, 15 represents 150 and likewise 25 represents 250 mm). We have placed a vertical scale on the narrow side-wall (away from the nozzle side) which will help to read the wave amplitude.

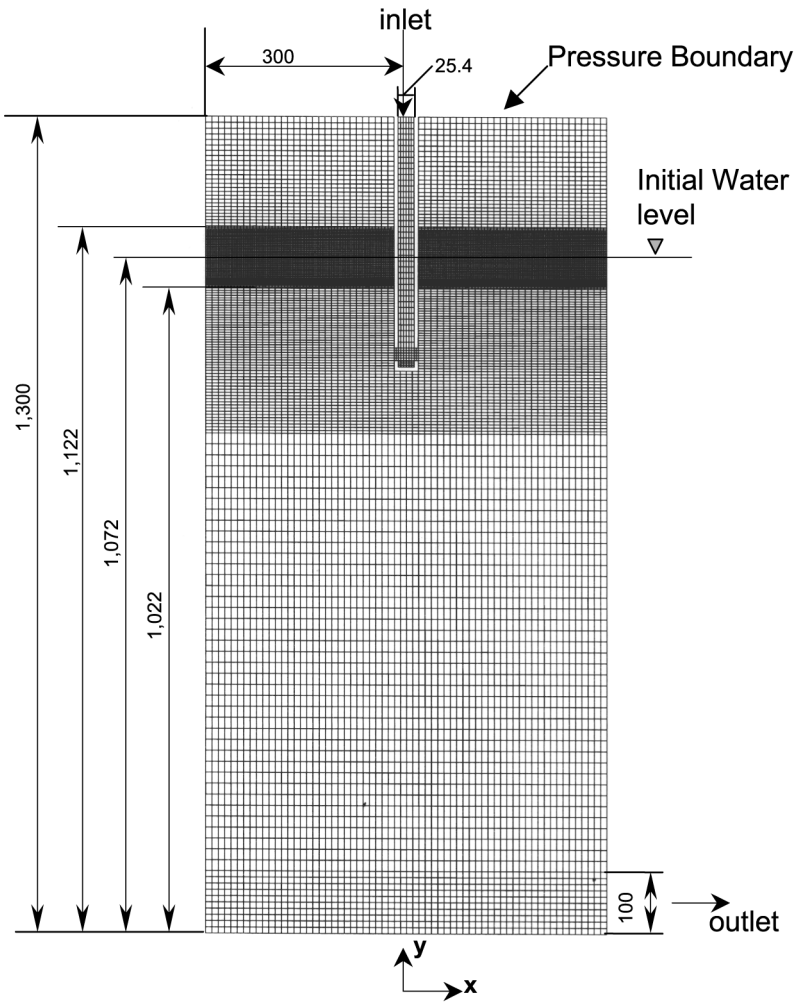

Note: All dimensions in mm

Source: Gupta & Lahiri

Figure 7.
Computational domain with grid arrangements for the simulation of experiment

Figure 9 shows five frames (a-e) shot with an interval of 0.04 s just at the time of entrapment of air bubble in the experiment (but the exact time of entrapment is not mentioned in the work of Gupta and Lahiri). It can be observed that frames 9(d) and (e) from the experimental snapshot match closely with that of the frames 8(d) and (e) of the present computation. In frame "d" of Figures 8 and 9 the surface is about to break and about to entrap an air bubble at the trough of the free surface and the air bubble is entrapped in the next moment, which is shown in frame "e" of both experimental and numerical investigations. The air

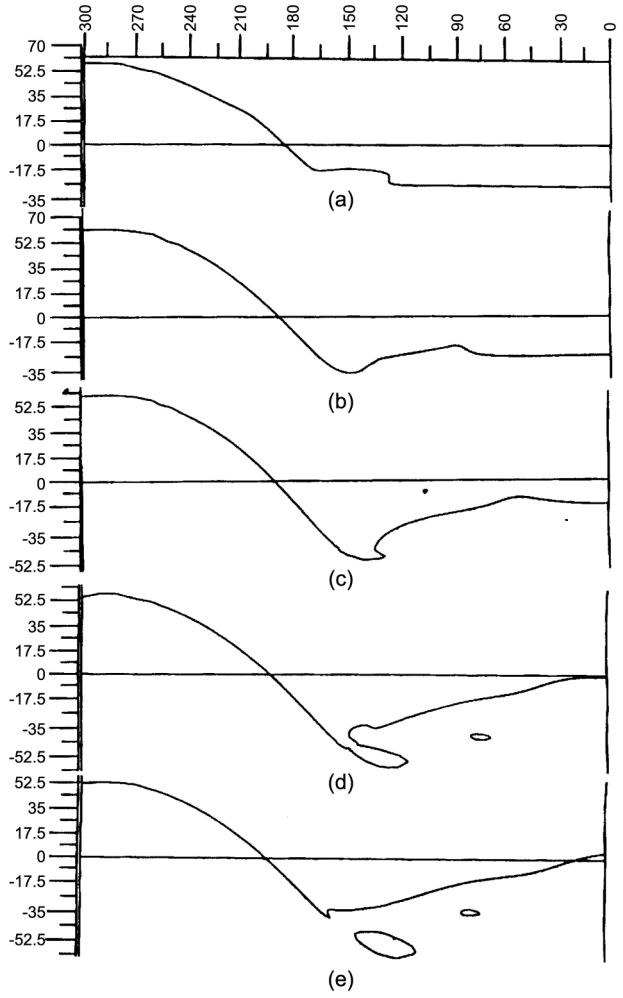

Figure 8.
Computed shape of the free surface at an interval of 0.04 s, starting time = 1.2 s, a comparison with the experimental observation showing bubble entrapment

bubble is seen as a large white patch just close to the trough of the free surface in frame "e" of Figure 9 and in Figure 8(e) it is seen to be a close contour having mass fraction of 0.5.

They had observed entrapment of air bubble by the free surface near the trough, which can be seen from the present computation of free surface also. They report the free surface to be a transient one, as does the present computation. The average maximum wave amplitude has been reported to be 28 mm for their case while in the present computation we have done the simulation only up to 2 s just to capture the entrapment of air bubble. So the average wave amplitude of the present simulation cannot be compared with their experiment because the average amplitude in the experiment has been

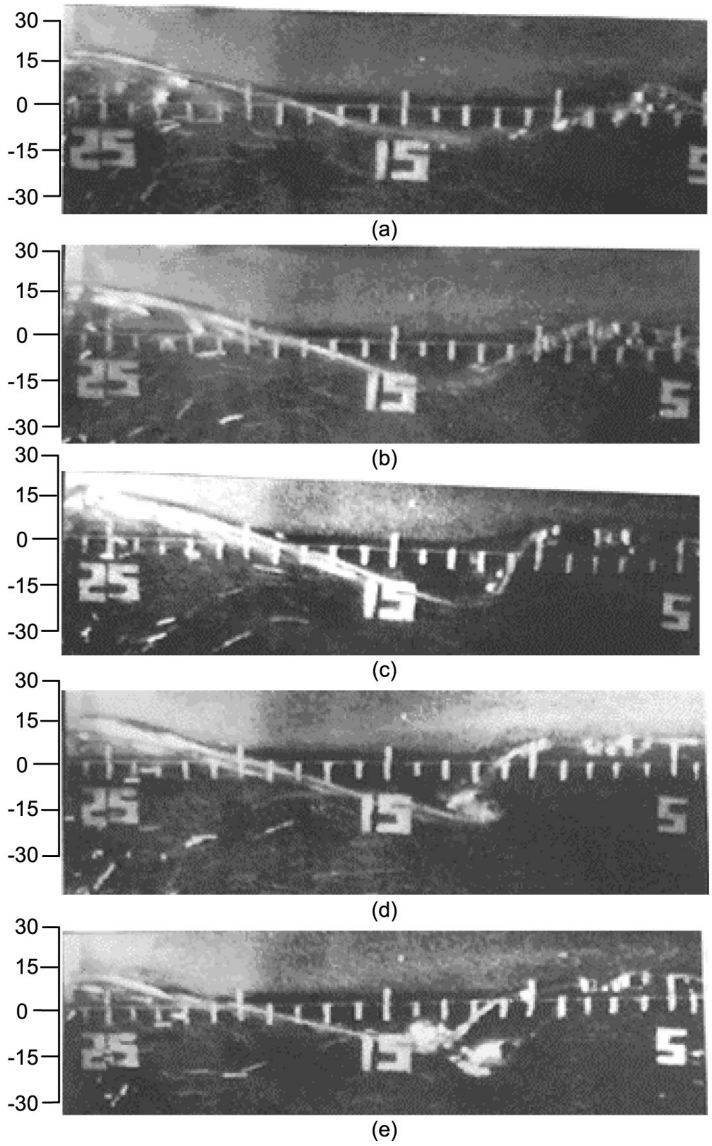

Figure 9.
Sequential photographs of the free surface at an interval of 0.04 s for a parallel port SEN with a port exit velocity of 1.94 m/s (Gupta and Lahiri)

computed over a long interval of time when the initial transience has completely died out. During the first 2 s of the computation, the wave amplitude will remain high and that will slowly decrease to a smaller value with the free surface randomly breaking and entrapping air bubbles the way it has been shown in Figure 6. Computing the average wave amplitude over a long period is extremely time-consuming for a numerical set-up for which effort has not

been given in that direction. However, looking at the location of the trough of the free surface and the place of bubble entrapment, it seems that the present computation is able to give the right trend in predicting the overall shape and entrapment of air bubble through a free surface.

Velocity field around the free surface

Figure 10 shows the velocity field around the free surface and the nozzle exit in the numerical simulation done for the experiment of Gupta and Lahiri. Figure 10(a) shows the flow field at $t = 1.2$ s along with the free surface described in it (this can be seen as a solid line in Figure 10(a), the horizontal solid line represents the initial liquid level). Figure 10(b) shows the free surface when it is just about to overturn and capture a bubble. It can be seen from Figure 10(a) and (b) that at the location of the trough there is a recirculating fluid packet just formed prior to the entrapment of an air bubble. Just after a while when the bubble is entrapped (in Figure 10(c), the free surface and the bubble can be seen), the recirculation disappears in the air side and the free surface pushes out the surrounding air to its right and the bubble is also pushed towards the nozzle due to the local convection present in the heavier fluid. This way the bubble travels little down into the heavier fluid and then it comes closer to the nozzle wall where it moves up to the free surface again and collapses on it. It must be marked from the figure that no bubble can travel to the left or towards the narrow side wall rather they are helped, because of the local flow field, to travel towards the nozzle and rise upward to the free surface again where they can collapse.

Grid independent free surface

In the present computation we have used a cell size of 1.85×1.85 mm near the free surface (Figure 5) to capture the free surface very sharp where we have studied the entrapment of bubbles along with its fragmentation and coalescence. In the numerical simulation done for the experiment of Gupta and Lahiri we have used two kinds of cell size, a coarser one with a size of 2.5×2.5 mm along with a finer one having a size of 1.25×1.25 mm to find out the effect of cell size on the free surface and bubble entrapment. It can be seen from Figure 11 that there is not much difference between the two free surfaces computed by the coarse and the fine cell at $t = 1.2$ s. Again at $t = 1.36$ s, a comparison between the coarse and the fine cell, in predicting the free surface along with an entrapment of the air bubble, can be seen from Figure 11(b). From the study of Figure 11, it can be concluded that a cell size of 2.5×2.5 mm near the free surface is well capable of predicting the free surface and bubble entrapment accurately when the inlet velocity is limited to about 3 m/s.

Conclusions

The numerical solution of the Navier-Stokes equations along with the mass and volume fraction conservation equations for both air and water has

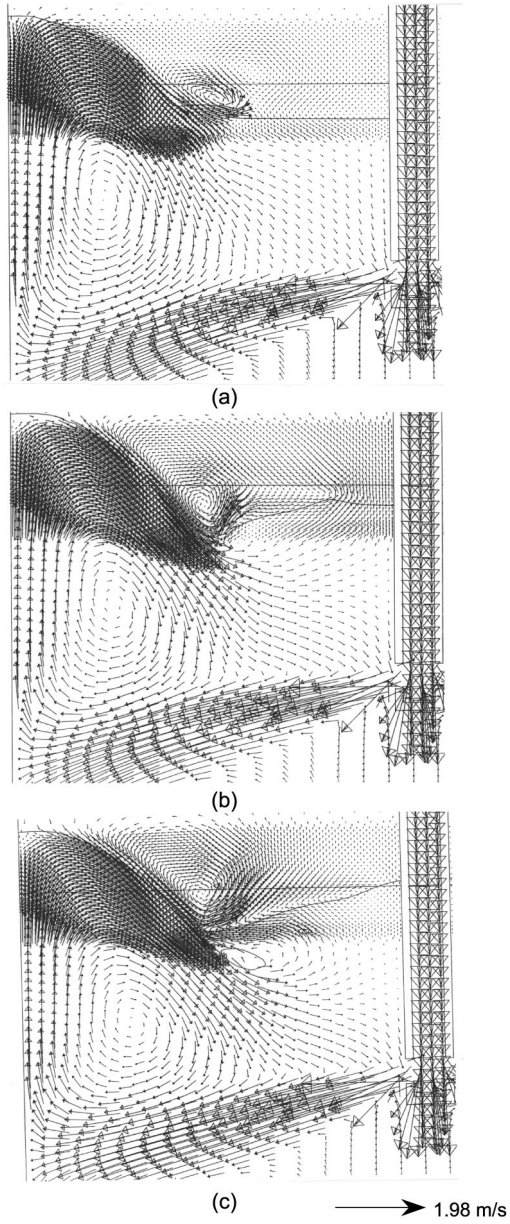

Figure 10.
Velocity field in the mold showing the free surface, (a) $t = 1.2$ s wave is about to be created, (b) $t = 1.32$ s, wave is about to break (c) $t = 1.36$ s, just after the entrapment of an air bubble

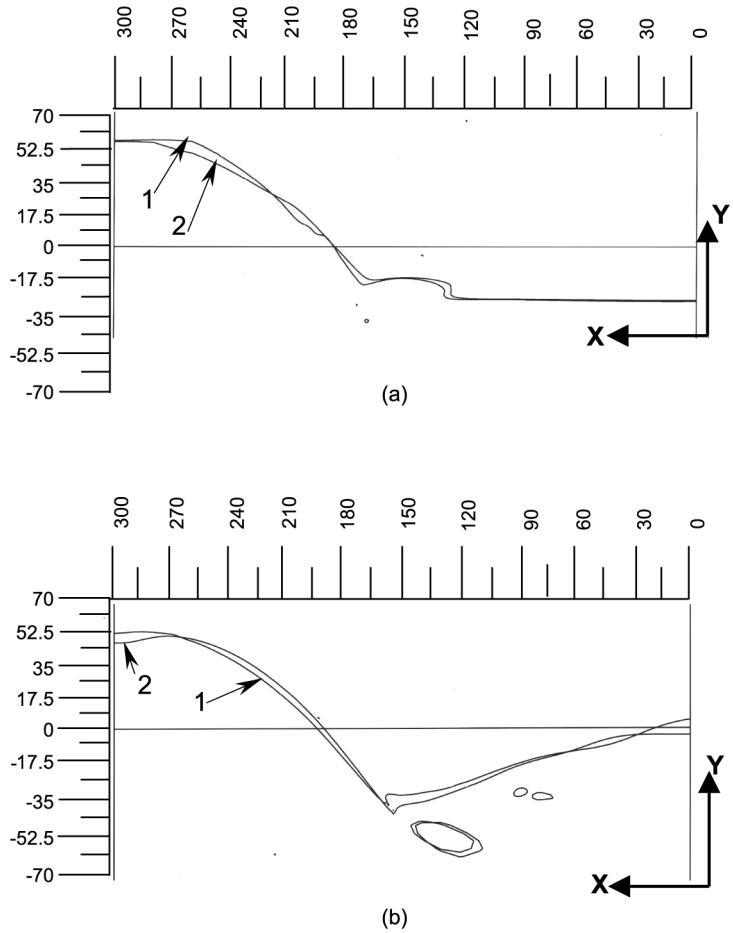

Figure 11.
Shape of the free surface at (a) $t = 1.2$ s, (b) $t = 1.36$ s and a comparison of the shape after making the cell size half in both x and y directions, (1) Cell size $= 2.5 \times 2.5$ mm, (2) cell size $= 1.25 \times 1.25$ mm

been shown to provide results for water flows in parallel and inclined port nozzles of a SEN fitted to a mold, which agree both qualitatively and to a large extent also quantitatively with experimental observations. It can be concluded that the free surface is transient in nature and never attains perfect steady state. The breaking of the free surface occurs randomly but the shape does not change very significantly after some time leaving the initial transience. The maximum wave amplitude of the free surface remains high at the start up and then gets fixed to a certain band within which it varies all the time. The present computation is able to predict the entrapment of air bubble and its subsequent fragmentation or coalescence within the mold, which has been also experimentally verified. It can also be concluded that a two-dimensional simulation for this purpose is good enough as far as the measurement of the maximum wave amplitude and

entrapment of air is concerned. However, if it is desired to observe the development of vortices on a free surface then a three-dimensional computation has to be undertaken at the expense of time.

References

Anagnostopoulos, J. and Bergeles, G. (1999), "Three dimensional modeling of flow and the interface surface in a continuous casting mold model", *Metall. Mater. Trans. B*, Vol. 30B, pp. 1095-105.

Andrzejewski, A., Kohler, K. and Pluschkell, W. (1992), "Model investigations on the fluid flow in continuous casting molds of wide dimensions", *Steel Res.*, Vol. 63 No. 6, pp. 242-6.

Brackbill, J.U., Kothe, D.B. and Zemaach, C. (1992), "A continuum method for modeling surface tension", *J. Comput. Phys.*, Vol. 1, pp. 335-54.

Comet User Manual (n.d.), ICCM Institute of Computational Continuum Mechanics GmbH, Hamburg, Germany, available at: www.iccm.de

Ferritti, A., Podrini, M. and Schino, Si G (1985), "Submerged nozzle optimization to improve stainless steel surface quality at Terni Steelworks", *Steelmaking Proc.*, Vol. 68, pp. 49-57.

Gupta, D. and Lahiri, A.K. (1992), "Water modeling study of the jet characteristics in a continuous casting mould", *Steel Res.*, Vol. 63 No. 5, pp. 201-4.

Gupta, D. and Lahiri, A.K. (1993), "Water modeling study of the surface disturbances in continuous slab caster", *Metall. Material. Trans. B*, Vol. 1, pp. 228-32.

Gupta, D., Subramanium, S. and Lahiri, A.K. (1991), "Study of fluid flow and residence-time distribution in a continuous slab casting mold", *Steel Res.*, Vol. 62 No. 11, pp. 496-500.

Jha Pradeep, K. and Dash Sukanta, K. (2002), "Effect of outlet positions and various turbulence models on mixing in a single, multi strand tundish", *Int. J. Num. Methods Heat Fluid Flow*, Vol. 12, pp. 560-84.

Lafaurie, B., Nardone, C., Scardovelli, R., Zaleski, S. and Zanetti, G. (1994), "Modelling merging and fragmentation in multiphase flows with SURFER", *J. Comput. Phys.*, Vol. 113, pp. 134-47.

Matsuhita, A., Isogami, K., Temma, M., Ninomiya, T. and Tsutsumi, K. (1988), "A mathematical model of solute redistribution during dendritic solidification", *Trans. Iron Steel Inst. Japan*, Vol. 28, pp. 531-4.

Muzaferija, S. and Peric, M. (1999), "Computation of free surface flow using interface-tracking and interface-capturing methods", in Mahrenholtz, O. and Markiewicz, M. (Eds), *Nonlinear Water Wave Interaction*,WIT Press, Southampton, Chap. 2, pp. 59-100.

Nakato, B.H., Ozawa, M., Kinoshita, K., Habu, Y. and Emi, T. (1984), "Factors affecting the formation of shell and longitudinal cracks in mold during high speed continuous casting of slabs", *Trans. Iron Steel Inst. Japan*, Vol. 24, pp. 957-65.

Panaras, G.A., Theodorrakakos, A. and Bergeles, G. (1998), "Numerical investigation of the free surface in a continuous steel casting mold", *Metall. Mater. Trans. B.*, Vol. 29B, pp. 1117-26.

Patankar, S.V. and Spalding, D.B. (1972), "A calculation procedure for heat, mass and momentum transfer in three-dimensional parabolic flows", *Int. J. Heat Mass Transfer*, Vol. 15, pp. 1787-806.

Qinglin, H.E. (1993), "Observation of vortex formation in the mold of a continuous slab caster", *Trans. Iron Steel Inst. Japan*, Vol. 33 No. 2, pp. 343-5.

Robertson, T., Moore, P. and Hawkins, R.J. (1986), "Computational flow model as aid to solution of fluid flow problems in the steel industry", *Ironmaking Steelmaking*, Vol. 13 No. 4, pp. 195-203.

Szekely, S. and Yadoya, R.T. (1972), "Physical and mathematical modeling of the flow field in the mold region in continuous casting system", *Metall. Trans.*, Vol. 3, pp. 2673-80.

Theodorrakakos, A. and Bergeles, G. (1998), "Numerical investigation of the interface in a continuous steel casting mold, water model", *Metall. Mater. Trans. B*, Vol. 29B, pp. 1321-7.

Thomas, B.G., Mika, L.J. and Najjar, F.M. (1990), "Simulation of fluid flow in a continuous slab casting machine", *Metall. Trans. B.*, Vol. 21, pp. 387-400.

Ubbink, O., (1997), "Numerical prediction of two fluid systems with sharp interfaces", PhD thesis, University of London.